

Quantum-Assisted Clustering Algorithms for NISQ-Era Devices

Samuel S. Mendelson,* Robert W. Strand,† Guy Oldaker IV,‡ and Jacob M. Farinholt§

*Strategic & Computing Systems Department
Naval Surface Warfare Center, Dahlgren Division
Dahlgren, VA*

(Dated: April 30, 2019)

In this article, we demonstrate how to view stoquastic adiabatic quantum computing from a purely graph-theoretic perspective, and then use this structure to design hybrid quantum-classical clustering algorithms. These algorithms require a number of qubits that is at most logarithmic in the size of the data, and appear to be more robust than their classical counterparts as noise is added to the data. Consequently, we believe that these algorithms will have great utility on NISQ-era adiabatic quantum computing devices.

I. INTRODUCTION

The noisy, intermediate scale quantum (NISQ) computing regime, a term first coined by Preskill in [1], refers to the computing regime we are expected to reside in for the next decade or so. NISQ computing assumes $\sim 50 - 100$ qubits and a universal, albeit imperfect, set of gates. We should not expect to realize quantum algorithms in this regime that will have an exponential computational improvement over existing classical algorithms. Nevertheless, it may be possible to construct NISQ-era quantum (or hybrid) algorithms that have some other performance advantage. In particular, there has been significant recent interest in the development of NISQ-era algorithms for machine learning. While the list of publications in this area is rapidly growing [2–10], well-known examples include the Quantum Approximate Optimization Algorithm (QAOA) [11–13] and the Variational Quantum Eigensolver (VQE) [14, 15]. For a more extensive review of research in the area of quantum machine learning, we refer the reader to [16].

Quantum algorithms that demonstrate an exponential advantage over classical algorithms often assume fault-tolerance. Because threshold theorems that admit fault-tolerant constructions only exist for circuit-based models, these models are generally pursued for scalable systems. However, because fault-tolerance cannot be assumed in the development of NISQ-era quantum algorithms, it is reasonable to treat adiabatic NISQ algorithms on equal footing as their circuit-based counterparts.

A particular subset of adiabatic quantum computing that has received much attention is one in which the problem Hamiltonian is *stoquastic*, that is, a Hamiltonian such that, when expressed in a predetermined, fixed basis, has the property that all of the off-diagonal elements are non-positive. Generally, we assume that the ground state is then measured in this fixed basis, although some

have considered more general scenarios in which the measurement basis can be adaptively varied [17]. If the measurement basis can be adaptively chosen, then Ref. [17] has shown that stoquastic adiabatic quantum computing can efficiently simulate quantum computing, and is hence universal.

If we utilize only a fixed measurement basis (hereinafter referred to as the “computational basis”), then with few exceptions [18, 19], it is believed that this restricted class of computations can be efficiently simulated classically. Nevertheless, stoquastic adiabatic algorithms may be able to demonstrate a significant performance advantage over certain existing classical algorithms, especially in the realm of machine learning, where quality and robustness are often more important performance parameters than run-time.

In what follows, we will view stoquastic adiabatic quantum computing from a graph-theoretic perspective. In this framework, we design hybrid quantum-classical clustering algorithms that require very few qubits and show a significant performance increase in quality over their classical counterparts. Consequently, we believe that these algorithms will have great utility on NISQ-era adiabatic quantum computing devices. We note that our approach is uniquely different from most previous adiabatic algorithms, as the quantum subroutine is not the solution to an optimization problem and the final Hamiltonian is not diagonal in the computational basis.

II. DEFINITIONS AND NOTATION

We begin with a graph $G = (V, E)$ with vertex set V and edge set $E \subset \binom{V}{2}$. In this paper, we consider undirected, weighted graphs with symmetric edge-weight functions. Let $u \in V$ be a vertex in G and $\omega : E \rightarrow \mathbb{R}^+$ be the edge-weight function. We define the degree of u as $d_u = \sum_{v \in V} \omega(u, v)$.¹ We define the *graph Laplacian*

* Samuel.Mendelson@navy.mil

† Robert.Strand@navy.mil

‡ Guy.B.Oldaker@navy.mil

§ Jacob.Farinholt@navy.mil

¹ When $\omega(u, v) = 1$ for all $(u, v) \in E$, d_u corresponds to the standard definition of degree.

of G , $L(G)$, as

$$L(G)_{uv} = \begin{cases} d_u & u = v \\ -\omega_{uv} & u \neq v \end{cases}. \quad (1)$$

Now let $W : V \rightarrow \mathbb{R}$ be a vertex-weight function. We write W as a diagonal matrix where $W_{uu} = W(u)$. If H is a stoquastic Hamiltonian, then we can decompose H as $H = L(G) + W$ for some graph G .² If $A \subset V$, we define

$$|\phi_A\rangle := |A|^{-1/2} \sum_{k \in A} |k\rangle \quad (2)$$

to be the equal superposition of all states corresponding to the vertices in A . We let $|\phi\rangle := |\phi_V\rangle$.

The graph Laplacian has two important properties that we will use throughout the rest of this paper. If $\lambda_0 \leq \lambda_1 \leq \dots \leq \lambda_n$ are the eigenvalues of the graph Laplacian $L(G)$, then $\lambda_0 = 0$ and the algebraic multiplicity of λ_0 is equal to the number of connected components of G . Second, if $\{G_i\}$ is the set of connected components of G , then $\{|\phi_{V_i}\rangle\}$ is an orthonormal basis for the eigenspace of λ_0 , where V_i is the vertex set of G_i . As we will consider systems in which the ground state is degenerate, we will denote the spectral gap of H as $\gamma = \lambda_j - \lambda_0$, where λ_j is the first eigenvalue strictly greater than λ_0 .

We often consider functions on graphs with the *Dirichlet boundary condition*. If $S \subset V$ and δS is the boundary of S , then $f : S \cup \delta S \rightarrow \mathbb{R}$ is said to have the Dirichlet boundary condition if $f(v) = 0$ for all $v \in \delta S$. We define Dirichlet eigenvalues of the Laplacian L as

$$\lambda_i^{(D)} = \min_{\substack{f \perp T_{i-1} \\ f|_{\delta S} = 0}} \frac{\langle Lf, f \rangle}{\langle f, f \rangle},$$

where T_j is the space spanned by the functions f_k that attain λ_k for $0 \leq k \leq j$. We call these f_j the Dirichlet eigenvectors corresponding to the Dirichlet eigenvalues. For a more detailed overview of Dirichlet eigenvalues and spectral graph theory, we refer the reader to [20].

III. GROVER'S ALGORITHM

Adiabatic Grover's algorithm on an n -state system consists of an initial and final Hamiltonian and a schedule $s(t)$. The initial Hamiltonian for Grover's is given by $H_I = \mathbb{I} - |\phi\rangle\langle\phi|$.³ Grover's final Hamiltonian is given by $H_{Grover} = \mathbb{I} - |m\rangle\langle m|$, where $|m\rangle$ is the state of interest

and the ground state of H_{Grover} . The quantum system is initialized as $|\phi\rangle$, the ground state of H_I , and the system is evolved according to $H(s) = (1-s)H_I + sH_{Grover}(s)$ where the schedule s is given by

$$s(t) = \frac{1}{2\sqrt{n-1}} \tan \left(2 \frac{\sqrt{n-1}}{n} \epsilon t - \arctan(\sqrt{n-1}) \right) + \frac{1}{2}, \quad (3)$$

with $s(t_i) = 0$, $s(t_f) = 1$, and ϵ determines a lower bound of the inner product between the final state of the evolution $|E_f\rangle$ and $|m\rangle$ given by $|\langle E_f | m \rangle|^2 \geq 1 - \epsilon^2$ [21].

Grover's algorithm can be generalized to a system in which there are multiple states of interest. Suppose in an n state system we are interested in measuring any of the states in the set $M = \{|m_i\rangle\}_i$. The initial Hamiltonian remains the same as H_I while the final Hamiltonian becomes $H_{Grover} = \mathbb{I} - \frac{1}{|M|} \sum_i |m_i\rangle\langle m_i|$. The schedule then changes to

$$s(t) = \frac{1}{2\sqrt{r-1}} \tan \left(2 \frac{\sqrt{r-1}}{r} \epsilon t - \arctan(\sqrt{r-1}) \right) + \frac{1}{2}, \quad (4)$$

where $r = n/|M|$.

Here, we give a graph-theoretic interpretation of Grover's algorithm on an n -state system. Grover's final Hamiltonian can be decomposed as $H_{Grover} = L(G) + W$ where G is the empty graph on n vertices and $W_u = 1 - \delta_{uv_m}$ where v_m corresponds with the state of interest $|m\rangle$. We embed G into a larger graph H with one more vertex v_n . The vertex v_n is connected to every other vertex except v_m . We can then recover Grover's system by imposing a Dirichlet boundary condition on v_n and considering the Dirichlet eigenvalues and eigenvectors of H . In practice, we can impose the Dirichlet boundary condition on v_n by restricting $L(H)$ to the vertices in G . We can see explicitly then, that this Dirichlet boundary condition will return H_{Grover} .⁴ The submatrix obtained by this restriction is called the *reduced Laplacian*. The vertices on which we impose the Dirichlet boundary condition will be called *marked vertices*. We use this method of marking vertices to give a generalization of adiabatic Grover's algorithm. See Figure 1 for the graph characterization of traditional Grover's algorithm.

A. Generalization of Adiabatic Grover's

Before we proceed, we state a simple but important structural lemma for the spectrum of a convex path through the space of Hermitian matrices. The proof is straightforward, and so we omit.

² When it is clear from context we will omit the dependence of L on G .

³ This is a standard initial Hamiltonian in many adiabatic algorithms.

⁴ Alternatively, we can impose the boundary condition by introducing a very large weight on v_n . This will force v_n to be approximately orthogonal to the ground state of $L(H)$. Intuitively, all vertices adjacent to v_n will be affected by this weight and will be pushed out of the ground state as well.

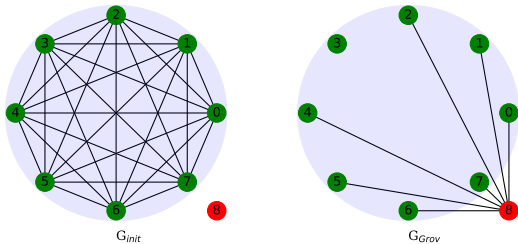


FIG. 1: The graphs G_{init} and G_{Grov} corresponding to the initial and final Hamiltonians, respectively, in Grover's search algorithm over an eight element data set, where the desired element is the state $|3\rangle$. The vertices in the shaded region correspond to elements of the unsorted database, while the outside red vertex acts as a “dummy” vertex. By deleting the row and column corresponding to the dummy vertex in both graph Laplacians, we obtain the initial and final Hamiltonians of adiabatic Grover's algorithm.

Lemma 1. *Let $H : [0, 1] \rightarrow \mathbb{H}$ be a path through the vector space, \mathbb{H} , of $(n \times n)$ Hermitian matrices, such that $H(s) = (1-s)H(0) + sH(1)$. Let A be the m -dimensional subspace of vectors that are eigenvectors of both $H(0)$ and $H(1)$ and $B = A^\perp$.*

- 1) *There exists an orthonormal basis $\{f_i\}_{i=0}^{m-1}$ for A such that f_i is an eigenvector of $H(s)$ for all $s \in [0, 1]$.*
- 2) *Let $\{\alpha_i\}_{i=0}^{n-m-1}$ be an eigenbasis of $H(0)$ for B and $\{\beta_i\}_{i=0}^{n-m-1}$ be an eigenbasis of $H(1)$ for B . The remaining eigenvectors and eigenvalues of $H(s)$ (those not in A) depend only on $\{\alpha_i\}$, $\{\beta_i\}$, and their corresponding eigenvalues.*

This lemma tells us that the change in the spectral gap in the convex evolution of Hermitian matrices is uniquely determined by the eigenvectors in which the initial and final Hamiltonians differ. Applying this lemma to adiabatic Grover's algorithm gives us the following corollary.

Corollary 2. *Let $M \subset [n]$ and $B = [n] \setminus M$ where M is a collection of states of interest. The non-constant spectrum and corresponding eigenvectors of Grover's algorithm depend only on the eigenvectors and eigenvalues $(f_0 = |\phi_M\rangle, \phi_0 = 0)$, $(f_1 = |\phi_B\rangle, \phi_1 = 0)$, $(e_0 = |\phi\rangle, \lambda_0 = 0)$, and $(e_1 = \mathcal{N}(|B||\phi_M\rangle - |M||\phi_B\rangle), \lambda_0 = 1)$, where \mathcal{N} is a normalization coefficient.*

Proof. The ground state of H_I , is $|\phi\rangle$ and has a ground energy of 0. The ground state of H_{Grov} is $|\phi_M\rangle$ and also has ground energy 0. The first excited states of both are $(n-1)$ -degenerate with a first-excited energy of 1. The intersection of subspaces of the first-excited states is

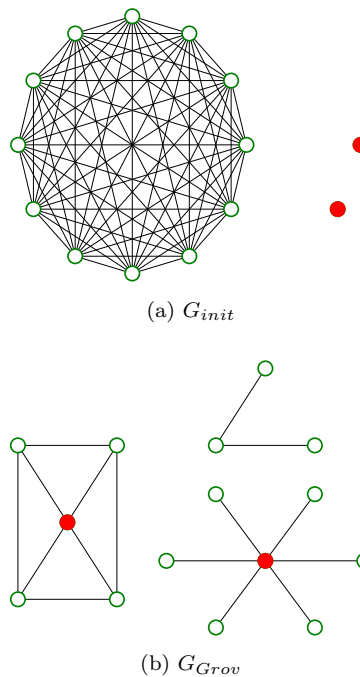


FIG. 2: The graphs for the initial (a) and final (b) Hamiltonians of a generalized adiabatic Grover's algorithm. The red (filled in) vertices are the “marked” vertices whose corresponding rows and columns are removed from the corresponding graph Laplacians to construct the reduced Laplacians that serve as the initial and final Hamiltonians. The ground state solution corresponds to the component in G_{Grov} that has no marked vertex.

an $(n-2)$ -dimensional subspace, and so H_I and H_{Grov} share an $(n-2)$ -dimensional eigenspace. The subspace on which they differ has an eigenbasis given by e_0 and e_1 for H_I and an eigenbasis of f_0 and f_1 for H_{Grov} as given above. Therefore, by the above lemma, the spectrum and eigenspace of $H(s) = (1-s)H_I + sH_{Grov}$ is determined only by (e_0, λ_0) , (e_1, λ_1) , (f_0, ϕ_0) , (f_1, ϕ_1) . \square

Using the above lemma and corollary, we give a graph-based generalization of adiabatic Grover's. Suppose now we have a graph of k connected components $\{G_i\}_{i=0}^{k-1}$ with $|V| = n$ and we are interested in finding a vertex in the m -th component, G_m with $|V_m| = n_m$. We choose a set of vertices V_d such that every vertex not in G_m is adjacent to exactly one vertex in V_d . We mark (impose the Dirichlet boundary condition on) the vertices in V_d and use the corresponding reduced Laplacian as our final Hamiltonian H_F . The initial Hamiltonian H_I has all eigenvectors of H_F except $f_0 = |\phi_{G_m}\rangle$ and $f_1 = |\phi_{\{G_i\}_{i \neq m}}\rangle$. The corresponding eigenvalues are $\lambda_0 = 0$ and $\lambda_1 = 1$ respectively. Therefore, while the spectra and eigenspaces of H_F and H_{Grov} are very different, by Lemma 1, the gap and ground state of this algorithm are equivalent to that of Grover's.

We see, then, that there are a large number of problem Hamiltonians that operate identically to the traditional adiabatic Grover’s algorithm when the same initial Hamiltonian is used. Consequently, we have significantly extended the range of representations that a Grover’s Oracle may utilize to present the problem to an adiabatic quantum computer. In what follows, we will show how this generalization of Grover’s (and extensions thereof) can be applied to a number of classical clustering problems.

IV. QUAC

In this section, we utilize the graph structure of stoquastic adiabatic algorithms to develop a quantum subroutine for various clustering algorithms. After evaluating the quantum subroutine, we then construct various hybrid clustering algorithms that utilize it, and compare their performance against classical counterparts. We call this class of algorithms *quantum assisted clustering*, or *QUAC* algorithms.

A. Quantum Cluster Indicator

Suppose we have a graph G with connected components $\{G_i\}$. The goal of the quantum cluster indicator, or *QCI*, subroutine is to find a representative from a connected component with no marked vertices. Classically, there are breadth and depth-first search algorithms that will give a partition of the graph into connected components. Now, in a less ideal setting, we may be interested in finding representatives of components of the graph that are well-connected while the components themselves are weakly-connected to each other, where breath/depth-first search will no longer work. This is a description of graph clustering and it is this setting in which we apply our algorithms. In what follows, a *cluster* will refer to a subset of a graph that is much more highly connected within itself than to another cluster. The goal of *QCI* is to find representatives from each cluster.

The subroutine itself is rather straightforward. Given a graph Laplacian and a set of vertices to “mark,” the quantum computer builds its problem Hamiltonian from the corresponding reduced Laplacian.⁵ We then adiabatically evolve our system accordingly, and measure the final ground state in the computational basis. If the graph has multiple components, then the ground state immediately prior to final measurement will be a superposition of basis states representing vertices from unmarked connected components. Consequently, measuring the final state will give you a representative from a different

connected component, that is, a different cluster, with certainty. If, however, the graph is connected, but its components are only weakly connected, then the ground state of the problem Hamiltonian will be a superposition of all states, but the states with the largest amplitudes will be those from unmarked weakly connected components. Consequently, measuring the ground state has a high probability of collapsing it onto a representative of a previously unmarked cluster. In Figure 4 we provide an example of how the probability amplitudes of the vertices in the ground state solution change with each iteration of *QCI* run over the five cluster dataset from Figure 3. We provide the pseudocode for *QCI* in Algorithm 1.

Algorithm 1 Samples vertex based on Dirichlet boundary conditions

```

1: function QCI ( $L, marks$ )
   Input: Laplacian  $L$ , set of marked vertices  $marks$ 
   Output:  $v_{meas}$ 
2:    $H_I \leftarrow \mathbb{I} - |\phi\rangle\langle\phi|$ 
3:    $|\psi(0)\rangle \leftarrow |\phi\rangle$ 
4:    $H_F \leftarrow$  reduced Laplacian  $L$  with marked vertices  $marks$ 
5:   Evolve system
6:    $v_{meas} \leftarrow$  Measurement
7: return  $v_{meas}$ 

```

In what follows, we evolve the system according to Grover’s schedule with one state of interest. In the ideal setting, Grover’s schedule is correct, although the number of states of interest will almost always be greater than one. However, as more edges are added between clusters, this schedule will become less correct. Because these algorithms are probabilistic in nature (and the ratio of states to interesting states will be greater than we assume), this does not appear to affect performance in a significant way. Recently, an optimal adiabatic path scheduler, the bashful algorithm, was developed in [22], assuming the existence of a gap-finding oracle. The gap-finding oracle for a large class of Grover-like stoquastic algorithms was explicitly constructed in the same reference. While our *QCI* algorithm does not lie within this class, it does appear to be very similar. We believe that the gap-finding oracle can be adapted and applied to our setting as well. With the bashful algorithm, we believe that there will be a slight quality increase. We leave that for further research.

As the connected components become less connected and more edges are added between clusters, the effect of marking a random vertex in the component becomes weaker, and in turn, the gap becomes smaller and occurs closer to the end of the path. This is unsurprising: as the clusters become less cluster-like, we should expect the challenge of identifying a representative of a given cluster to become more difficult. In what follows, we will show that adapting well-known classical clustering algorithms to include the *QCI* subroutine nevertheless significantly improves the quality of the algorithms.

⁵ For the purposes of this algorithm, “marking” a vertex corresponds to deleting the corresponding row and column in the graph Laplacian.

We apply our algorithm in two scenarios. First, as a seed initialization for an existing classical algorithm: k -means. We show that our initialization performs just as well as the current standard, $k++$, on well-behaved datasets and outperforms it on others. Second, we use our algorithm as the basis for a new unsupervised nearest-neighbor clustering algorithm. These quantum-assisted clustering algorithms, or *QUACs*, are a hybrid between quantum computation and existing classical algorithms, and give a demonstrable performance improvement over their existing counterparts.

B. q -means

The k -means algorithm [23] is a standard clustering algorithm that is simple but effective. Given a set of vector-data, the k -means algorithm will partition the set into k clusters. To begin, a set of k seeds is chosen at random from the data. Next, the distance between each data point and each seed is calculated. The data is partitioned into k sets based on the closest seed. The centroid of each cluster is calculated as the average of the points in each cluster. Using these centroids, the data is partitioned again with the centroids as the new seeds. This process is repeated until either there is no update to the centroids or a maximum number of iterations is reached.

The goal of this algorithm is to minimize the inertia, that is, the sum of square distances to the centroids of each cluster. However, it is very sensitive to the initial choice of seeds and will often find a local minimum of inertia. In addition, if the initial seeds are poorly chosen, the algorithm may require a large number of iterations.

To combat these problems, a “smarter” seeding algorithm has been developed [24]. Known as $k++$, this seeding algorithm is based on the idea that cluster centers should be spaced far apart. First, a point is chosen at random to be the first seed. Next, the distance between the first seed and every other point is calculated. Using the normalized distances as a probability distribution, the next point is chosen. This process is repeated until all k seeds are chosen. The rest of the k -means algorithm remains unchanged. While there is a higher computation cost up-front, it has been shown that this initialization reduces the number of iterations required and is an overall reduction in computation. Empirically, the solutions tend to have better inertia as well. Even with these improvements, $k++$ will still produce poor results if the clusters are not spherical Gaussians with similar variation and density. As we will see, the solution that minimizes the inertia is not always the “correct” solution, and so a more in-depth analysis is needed. We will show how to use our QCI subroutine to generate seeds for the k -means algorithm and show that our seeds give a performance on par with $k++$ for well-behaved data and a demonstrable performance improvement for a certain class of data.

We note that an adiabatic initialization algorithm for k -means was developed previously in Ref. [?]; how-

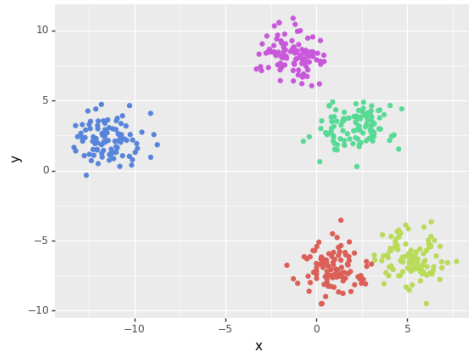


FIG. 3: The Five Cluster dataset, correctly partitioned.

ever the amplitudes of the ground state in that algorithm reproduce the probability amplitudes in the $k++$ algorithm, and consequently its ability to accurately cluster will be equivalent to that of $k++$. Our “ q -means” algorithm, on the other hand, will use QCI as a seed initialization for k -means. Since QCI requires graph data, we must first convert the vector data typically used in k -means into something usable. There are a number of standard techniques for transforming vector data into graph data. These include, but are not limited to, ϵ -balls, k -nearest-neighbors, kernel functions, and similarity measures. Countless papers have been written on the best techniques for converting vector data to graph data, and choosing the correct method is often as much an art as it is a science. The method of choosing the appropriate technique lies far outside the scope of this paper, and we refer the reader to, e.g., Ref. [25] and references therein for a more detailed introduction to this area.

To simulate our algorithm we use a numeric integrator on the time-dependant Schrödinger’s equation

$$i\hbar \frac{d}{dt} |\phi(t)\rangle = H(t) |\phi(t)\rangle, \quad (5)$$

where for simplicity, we set $\hbar = 1$. To facilitate computation, in our analysis we will use the ϵ -ball method throughout. Each point in the data set will be a vertex in our graph. For a prescribed ϵ , two points will have an edge between them if their Euclidean distance is less than ϵ . After the graph is constructed, outlier removal is performed, and then the corresponding graph Laplacian is constructed. The Laplacian for an ϵ -ball graph will have only 0’s and -1’s in the off-diagonal entries and, depending ϵ , will ease computation. We initialize our seeds on a subset of the data. This is done, again, to make computation more tractable. Once the seeds are chosen, we use k -means on the whole dataset. We note that even using a subset of the data to initialize, we still obtain performance on par with $k++$. All figures and results use ten percent of the original dataset for simulation with a sampling rate of twenty times the number of data points.

Once we construct the Laplacian for the data, we run

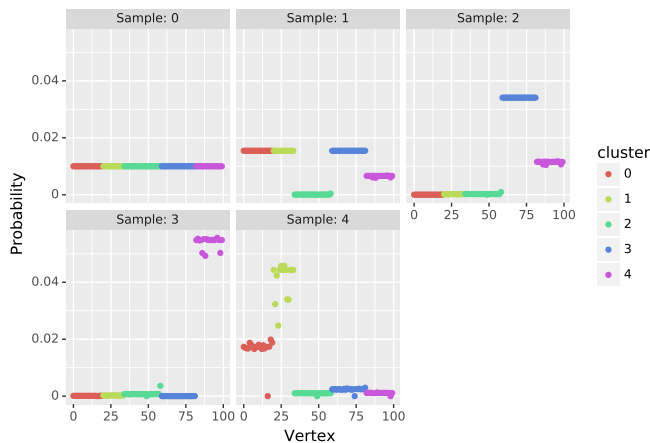


FIG. 4: An example of the change in probability amplitudes associated with each vertex in the ground state solution as we run QCI to find (and consequently mark) a representative of each cluster in the Five Cluster dataset.

QCI k times to obtain a representative of each cluster. While these points are representatives of the clusters, they are not necessarily good representatives of the cluster centers. In order to get a good approximation of the cluster center of the first cluster, we remove the mark associated with the first cluster and run QCI m many times (the sampling rate m is fixed at the beginning of the algorithm). QCI will return different representatives of the first cluster after each run. We average the data points associated with these vertices and use this for our initial centroid for the first cluster. We repeat this process for each of the k clusters. The pseudocode for q -means is provided in Algorithm 2.

Algorithm 2 Returns seed initialization for k -means

```

1: function  $q$ -means ( $X, L, k, m$ )
   Input: data set  $X$ , Laplacian of data  $L$ , number of clusters  $k$ , number of measurements for each cluster  $m$ 
   Output: seed initializations  $\{c_n\}_{n=1}^k$ 
2:    $v_1 \leftarrow$  vertex chosen uniformly at random
3:   for  $i \in [k - 1]$  do
4:      $v_{i+1} \leftarrow$  QCI ( $L, \{v_n\}_{n=1}^i$ )
5:   end for
6:   for  $i \in [k]$  do
7:     for  $j \in [m]$  do
8:        $u_j \leftarrow$  QCI ( $L, \{v_n\}_{n \neq i}$ )
9:     end for
10:     $c_i \leftarrow \frac{1}{m} \sum_n x_{u_n}$ 
11:  end for
12: return  $\{c_n\}$ 

```

We simulate q -means on two different datasets. The first is a set of points chosen from five circular Gaussian distributions, which we denote as the five cluster dataset (see Fig. 3). The $k++$ initialization performs

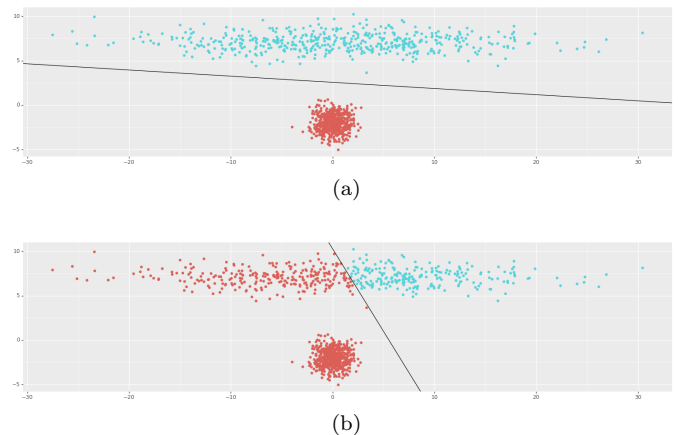


FIG. 5: The Elliptical dataset clustered (a) correctly, and (b) incorrectly. The second incorrect partition identified in Table I is the mirror image of the partition of (b).

| | Inertia | $ S_w $ |
|--------------------|------------|-----------------|
| Correct | 47,194.898 | 44,519,995.441 |
| Incorrect 1 | 39,503.416 | 257,968,951.423 |
| Incorrect 2 | 42,489.978 | 278,934,320.164 |

TABLE I: Comparison between the inertia and determinant criterion for the three solutions of k -means on the elliptical data set, given an optimal choice of ϵ .

extremely well on this type of data. The next dataset is a set of points chosen from two Gaussians; one of which is circular and one of which is elliptical (the variance in the x -direction is twice the variance in the y -direction) which we call the elliptical dataset (see Fig. 5). This dataset is particularly difficult for $k++$ (and the random initialization) to cluster “successfully.” By success, we mean the algorithm partitioned the dataset according to those clusters we visually distinguish. The inertia of the “correct” clustering of the elliptical dataset does not achieve the global minimum of the inertia. Because the k -means algorithm optimizes over inertia, a successful k -means will produce a solution with the minimum inertia. We therefore measure our clustering solutions with the *determinant criterion*, which is the determinant of the within-cluster scatter matrix.⁶ As we see in Table I, while the inertias of the three solutions are similar, the determinant criterion for the correct solution is an order of magnitude smaller.

Because we have introduced a new parameter, ϵ , we first show how ϵ affects the performance of q -means. As we can see in Figure 6, there is a wide range of ϵ ’s for which q -means has a higher probability of success over

⁶ Inertia is the trace of the within-cluster scatter matrix.

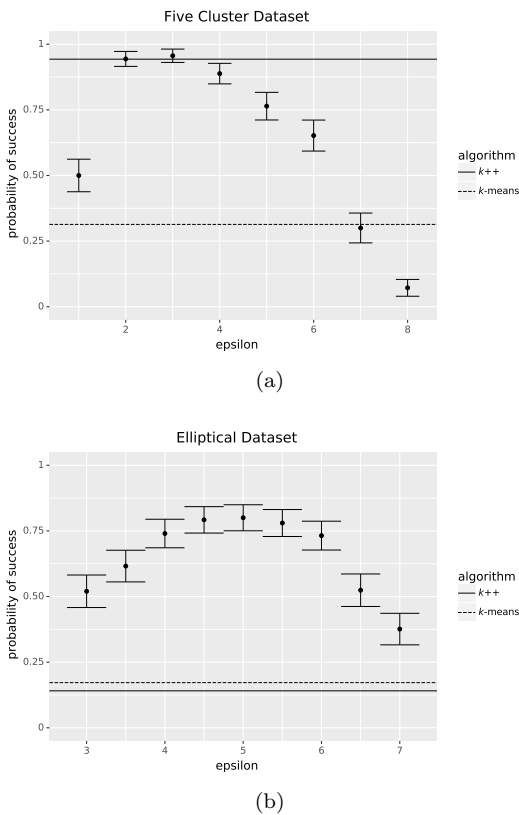


FIG. 6: A plot of the probabilities of success of q -means for various choices of ϵ in our construction of ϵ -balls for (a) the Five Cluster dataset and (b) the Elliptical dataset.

both k -means and $k++$ for the elliptical dataset. Conversely, on the five cluster dataset, there is a very small range in the choice of ϵ that returns a similar success probability as $k++$. Consequently, it is clear that a good estimate for ϵ is important, especially on highly idealized cluster data. The reason for wide variance in performance of q -means as we vary ϵ is that, when ϵ is too small, the corresponding graph will have more connected components than the number of clusters, whereas when ϵ becomes too large, the spectral evolution in the adiabatic subroutine begins to diverge from that of Grover’s. Table II summarizes the success rate and the number of iterations required for each dataset, given an optimal choice of ϵ . We note that the success probabilities would improve with high ϵ if it were possible to efficiently determine the optimal schedule, e.g. by extending the recently developed “bashful algorithm” [22] to this more general scenario.

C. q -nn

The l -nearest neighbor algorithm is a simple but effective algorithm for deciding how to associate new data to existing clusters. Suppose we begin with a labeled

| Algorithm | Success Rate | # Iterations when Successful | # Iterations when Failed |
|---------------------|--------------|------------------------------|--------------------------|
| Five Cluster | | | |
| q -means | 95.6% | 1.749 ± 0.791 | 6.000 ± 3.521 |
| $k++$ | 94.3% | 2.055 ± 0.634 | 5.319 ± 2.702 |
| random | 31.36% | 3.361 ± 1.061 | 6.244 ± 2.843 |
| Elliptical | | | |
| q -means | 80.0% | 1.575 ± 0.905 | 9.300 ± 1.529 |
| $k++$ | 14.58% | 1.851 ± 1.087 | 6.471 ± 2.296 |
| random | 17.2% | 2.155 ± 1.046 | 6.798 ± 2.319 |

TABLE II: Performance of each of the three initialization variants of k -means on the Five Cluster and Elliptical data sets with optimal choice of ϵ .

dataset with each point labeled as being in one of k clusters. Given a new point v , our goal is to assign v to one of the k clusters. The l -nearest neighbor algorithm chooses which cluster to associate to v by determining the clusters associated with the l nearest data points. The point v is assigned to a cluster based on a majority vote of these l points.⁷ In what follows, we develop a quantum initialization for the nearest neighbor algorithm, which we call q -nn. This initialization uses QCI to make an initial cluster estimation, and then uses the nearest-neighbor algorithm to partition the rest of the data.

Algorithm 3 Returns cluster labels for data points

```

1: function  $q$ -nn ( $L, k, m$ )
   Input: Laplacian  $L$ , number of clusters  $k$ , number of
   measurements for each cluster  $m$ 
   Output: label data  $\{u_n^1\}, \{u_n^2\}, \dots, \{u_n^k\}$ 
2:    $u_1^1 \leftarrow$  vertex chosen uniformly at random
3:   for  $i \in [k - 1]$  do
4:      $u_1^{i+1} \leftarrow$  QCI ( $L, \{u_n^i\}_{n=1}^i$ )
5:   end for
6:   for  $i \in [m]$  do
7:     for  $j \in [k]$  do
8:        $u_{i+1}^j \leftarrow$  QCI ( $L, \{u_1^i\}_{i \neq j}$ )
9:     end for
10:  end for
11: return  $\{u_n^1\}, \{u_n^2\}, \dots, \{u_n^k\}$ 

```

We begin with a set of vector data, a value k for the number of clusters, and a value m for the number of measurements we will perform for each cluster. Taking a subset of the data, and, using a prescribed ϵ for ϵ -balls, we create the graph Laplacian, L . Again, we take a subset of the data in order make simulating the system more manageable. However, we see, even using only a subset

⁷ There are different methods for dealing with ties. Usually though, they are broken arbitrarily.

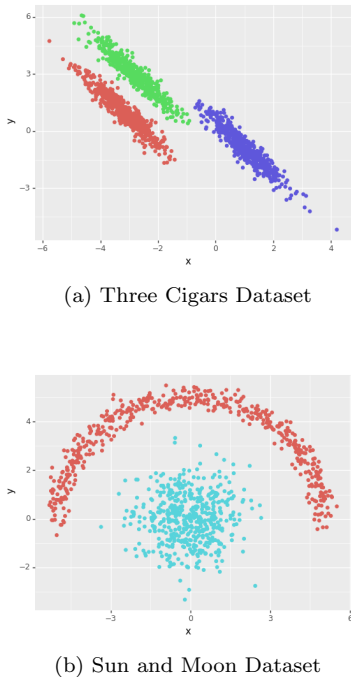


FIG. 7: Images of the correctly clustered (a) Three Cigars dataset and the (b) Sun and Moon dataset used to test q -nn.

of the data provides good results after applying the nearest neighbor algorithm. Similarly, while any method of graph construction can be used, ϵ -balls are used here to make simulation time tractable. The q -nn initialization proceeds similarly to the q -means initialization. The QCI algorithm is run k times to obtain a representative for each of the k clusters. For the j -th cluster, we mark all but the j -th representative and run QCI m times. Each of these measured vertices is labeled as being in cluster j . Finally, we perform the l -nearest neighbor algorithm on any unlabeled data (or in our case the rest of the data set) to finish clustering the data.

We test q -nn on two datasets, shown in Figure 7. The first dataset consists of data drawn from three anisotropic Gaussians (the *Three Cigars*). The second dataset is a half circle and a circular Gaussian (the *Sun and Moon*). As a measure of performance, we use the *adjusted rand index* between the cluster solution and the data's true labels.⁸ We compare q -nn to Laplacian spectral clustering, which also uses graph data and requires an input for the number of clusters expected. We note, however, that Laplacian spectral clustering works only over connected graphs, so in order to compare the two algorithms, thinned samples and choices of ϵ that returned graphs

with multiple connected components were removed from the spectral analysis. While q -nn works even when the graph has multiple connected components, we nevertheless are able to compare these algorithms for the same parameters when Laplacian spectral clustering is able to be utilized.

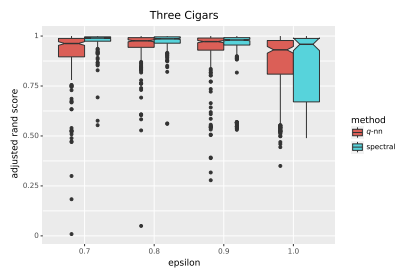
The box plots in Figure 8 compare the results of the q -nn algorithm against the Laplacian spectral clustering algorithm for various ϵ 's. We see that q -nn works extremely well on these datasets, with an average performance similar to spectral clustering on both datasets, albeit with a larger variance for most ϵ 's. The wider variance is due in part to the fact that we restricted ourselves to considering only connected graphs. The box plots also indicate that the performance of q -nn is influenced more by the choice of ϵ and the initial mark than the schedule, which is likely sub-optimal since the underlying graph structure diverges from that of the generalized Grover's algorithm. We believe that the reason why this choice of schedule (i.e. Grover's) still performs well is due to the cluster assignment process used by q -nn. This is done via a majority vote using the ground state vectors resulting from marking vertices. When using a sub-optimal schedule, the relative magnitudes of the different vectors used for cluster assignment maintain the same relationship between each other as those from the optimal case. So in the case of two clusters, the optimal schedule may give the probabilities of a vertex being in cluster 1 and 2 as 0.9 and 0.1 respectively, while the sub-optimal schedule may yield 0.7 and 0.3. Thus, while the amplitudes corresponding to the sub-optimal schedule may not be as large as those for the optimal case, on average the resulting assignments agree. This becomes particularly apparent when the sampling rate is sufficiently high, and explains why q -nn performs as well as spectral clustering on average, albeit with larger variance for certain values of ϵ .

V. CONCLUSION

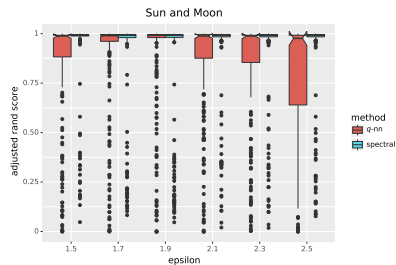
In conclusion, using the graph structure of stoquastic Hamiltonians, we have shown that it is possible to frame adiabatic Grover's algorithm in a graph-theoretic context, providing a straightforward path to generalizing Grover's to more complex problem Hamiltonians.

Additionally, we used the graph structure on these problem Hamiltonians to develop several hybrid quantum clustering algorithms that require a number of qubits that is logarithmic in the size of the data (n data points are enumerated by $\log_2(n)$ qubits). These algorithms exhibited competitive clustering performance with established techniques and, in the case of q -means, outperformed its classical counterpart, $k++$. Moreover, we demonstrated in our simulations that the quantum subroutine tends to provide good k -means initializations when run over only a small sample of the full data set. Both of these algorithms worked surprisingly well, even

⁸ The adjusted rand index is a measure of agreement between two partitions. A score of 1 represents a perfect match between the two partitions while a score of 0 represents a random labeling.



(a) Three Cigars Dataset box plots



(b) Sun and Moon Dataset box plots

FIG. 8: Box plots of ϵ vs. adjusted rand scores (ars) for q -nn (red) and spectral clustering (blue) for (a) the Three Cigars dataset and (b) the Sun and Moon dataset, over various ϵ 's.

though the schedule used in the adiabatic subroutine was often sub-optimal. Consequently, it is believed that these algorithms will be a particularly useful application of near-term quantum computers. While we only provided two algorithms in the QUAC suite in this paper, we believe that these ideas can be extended to other hybrid clustering algorithms.

The clustering algorithms we provided can likely be optimized further with better sampling rates, choice of initial mark, and optimized scheduling. In particular, we operated under the assumption that data sets to be clustered have an underlying graph structure similar to that of our generalized Grover's algorithm. Consequently, we ran QCI using the optimal Grover schedule. On abnormally shaped clusters the true optimal schedule tends to diverge from Grover's. However, making the schedules tight (for example with the bashful adiabatic algorithm [22]) can significantly improve overall algorithmic performance.

ACKNOWLEDGMENTS

This project was funded through Naval Surface Warfare Center, Dahlgren Division (NSWCDD) Navy Innovative Science and Engineering (NISE) program. The authors are particularly grateful for useful discussions and insights provided by Dave Marchette and the rest of the members of the AM&DA group.

-
- [1] J. Preskill, *Quantum* **2**, 79 (2018).
 - [2] V. Dunjko, Y. Ge, and J. I. Cirac, *Phys. Rev. Lett.* **121**, 250501 (2018).
 - [3] E. Farhi and H. Neven, "Classification with quantum neural networks on near term processors," (2018), arXiv:1802.06002.
 - [4] E. Farhi, J. Goldstone, S. Gutmann, and H. Neven, "Quantum algorithms for fixed qubit architectures," (2017), arXiv:1703.06199.
 - [5] A. Kandala, A. Mezzacapo, K. Temme, M. Takita, M. Brink, J. M. Chow, and J. M. Gambetta, *Nature* **549**, 242 EP (2017).
 - [6] W. Huggins, P. Patil, B. Mitchell, K. B. Whaley, and E. M. Stoudenmire, *Quantum Science and Technology* **4**, 024001 (2019).
 - [7] V. Havlicek, A. D. Croles, K. Temme, A. W. Harrow, A. Kandala, J. M. Chow, and J. M. Gambetta, "Supervised learning with quantum enhanced feature spaces," (2018), arXiv:1804.11326.
 - [8] M. Schuld, A. Bocharov, K. Svore, and N. Wiebe, "Circuit-centric quantum classifiers," (2018), arXiv:1804.00633.
 - [9] A. W. Cross, G. Smith, and J. A. Smolin, *Phys. Rev. A* **92**, 012327 (2015).
 - [10] C. M. Wilson, J. S. Otterbach, N. Tezak, R. S. Smith, G. E. Crooks, and M. P. da Silva, "Quantum kitchen sinks: An algorithm for machine learning on near-term quantum computers," (2018), arXiv:1806.08321.
 - [11] E. Farhi, J. Goldstone, and S. Gutmann, "A quantum approximate optimization algorithm," (2014), arXiv:1411.4028.
 - [12] E. Farhi, J. Goldstone, and S. Gutmann, "A quantum approximate optimization algorithm applied to a bounded occurrence constraint problem," (2014), arXiv:1412.6062.
 - [13] E. Farhi and A. W. Harrow, "Quantum supremacy through the quantum approximate optimization algorithm," (2016), arXiv:1602.07674.
 - [14] A. Peruzzo, J. McClean, P. Shadbolt, M.-H. Yung, X.-Q. Zhou, P. J. Love, A. Asuru-Guzik, and J. O'Brien, *Nature Communications* **5** (2014), 10.1038/ncomms5213.
 - [15] J. R. McClean, J. Romero, R. Babbush, and A. Aspuru-Guzik, *New Journal of Physics* **18**, 023023 (2016).
 - [16] J. Biamonte, P. Wittek, N. Pancotti, P. Rebentrost, N. Wiebe, and S. Lloyd, *Nature* **549**, 195 EP (2017).
 - [17] K. Fujii, "Quantum speedup in stoquastic adiabatic quantum computation," (2018), arXiv:1803.09954.
 - [18] M. B. Hastings, *Quantum Info. Comput.* **13**, 1038 (2013).
 - [19] M. Jarret, S. P. Jordan, and B. Lackey, *Phys. Rev. A* **94**, 042318 (2016).
 - [20] F. R. K. Chung, *Spectral Graph Theory* (American Mathematical Society, 1997).
 - [21] J. E. Avron, M. Fraas, G. M. Graf, and P. Grech, *Phys. Rev. A* **82**, 040304 (2010).
 - [22] M. Jarret, B. Lackey, A. Liu, and K. Wan, "Quantum adiabatic optimization without heuristics," (2018),

arXiv:1810.04686.

- [23] S. Lloyd, IEEE Transactions on Information Theory **28**, 129 (1982).
- [24] D. Arthur and S. Vassilvitskii, in *Proceedings of the Eighteenth Annual ACM-SIAM Symposium on Discrete Algorithms*, SODA '07 (Society for Industrial and Applied Mathematics, Philadelphia, PA, USA, 2007) pp. 1027–1035.
- [25] S. I. Daitch, J. A. Kelner, and D. A. Spielman, in *Proceedings of the 26th Annual International Conference on Machine Learning*, ICML '09 (ACM, New York, NY, USA, 2009) pp. 201–208.